

# N-polar GaN/AlGaN/GaN high electron mobility transistors

Siddharth Rajan<sup>a)</sup>

*Electrical and Computer Engineering Department, University of California, Santa Barbara, California 93106*

Alessandro Chini

*Department of Information Engineering, University of Modena and Reggio Emilia, I-41100 Modena, Italy and INFN, University of Modena and Reggio Emilia, I-41100 Modena, Italy*

Man Hoi Wong

*Electrical and Computer Engineering Department, University of California, Santa Barbara, California 93106*

James S. Speck

*Materials Department, University of California, Santa Barbara, California 93106*

Umesh K. Mishra

*Electrical and Computer Engineering Department, University of California, Santa Barbara, California 93106*

(Received 9 April 2007; accepted 3 July 2007; published online 17 August 2007)

We describe the development of N-polar GaN-based high electron mobility transistors grown by N<sub>2</sub> plasma-assisted molecular beam epitaxy on C-face SiC substrates. High mobility AlGaN/GaN modulation-doped two-dimensional electron gas channels were grown, and transistors with excellent dc and small-signal performance were fabricated on these wafers. Large-signal dispersion was observed, and the trap states responsible for this were identified, and layer designs to remove the dispersive effects of these traps were demonstrated. Finally, an AlGaN-cap layer was used to reduce gate leakage in these devices, and a low-dispersion high breakdown voltage device was achieved. This detailed study of dispersion and leakage in N-polar GaN-based transistors establishes a technological base for further development of field effect devices based on N-polar III-nitrides.

© 2007 American Institute of Physics. [DOI: [10.1063/1.2769950](https://doi.org/10.1063/1.2769950)]

## I. INTRODUCTION

III-nitrides can be grown in wurtzite and zinc-blende phases, with the most commonly used and stable crystal phase being wurtzite. Due to the inversion asymmetry along the *c* axis in the wurtzite phase, structures grown along the (0001) and (000 $\bar{1}$ ) directions have different surface properties and growth kinetics. Also, nitrides exhibit high spontaneous or piezoelectric polarization fields that are oriented along the *c* direction. Due to polarization effects, the band diagrams and electrostatics of structures grown along the Ga polar, or (0001) direction, are very different from electrostatics along the N-polar, or (000 $\bar{1}$ ) direction.

With a few exceptions,<sup>1,2</sup> most research in III-nitride optoelectronic and electronic devices in the past has focused on materials and heterostructures grown in the Ga-polar direction. However, the reversed direction of polarization in N-polar nitride structures can be used in many device structures. The direction of polarization fields is especially advantageous for enhancement mode transistors and highly scaled GaN transistors. In addition, the more reactive nature of the N-polar surface makes it suitable for sensor applications. Since epitaxial growth is a strong function of the surface of the material, the growth kinetics of N-face and III-face nitrides are very different. It has been shown that N-polar InN

can be grown at much higher temperatures on N-polar surfaces.<sup>3</sup> Also Mg doping can be carried out without problems of surface polarity inversion on the N-polar surface. The availability of N-polar technology therefore provides greater flexibility in applying nitride semiconductors.

This paper is organized as follows. N-polar field effect transistors (FETs) grown by N<sub>2</sub> plasma-assisted molecular beam epitaxy (MBE) on C-face SiC using abrupt GaN/AlGaN/GaN heterostructure layers are described in Sec. II. These devices were found to have good dc and small-signal performance but suffered from current collapse under large-signal pulsed conditions. In Sec. III, we propose that the origin of this dispersion is donorlike traps, and report on the design and performance of a device structure that eliminates the dispersion. Finally, in Sec. IV, the use of an AlGaN cap to reduce the gate leakage in these transistors is demonstrated, and a device with low dispersion and gate leakage is shown.

## II. GaN/AlGaN/GaN MODULATION-DOPED FETS

### A. Growth and fabrication

AlGaN/GaN heterostructures were grown on C-face SiC substrates using optimized two-step GaN buffer layers<sup>4,5</sup> to realize a high mobility two-dimensional electron gas (2DEG) for transistor operation. The epitaxial layer structure consisted of an undoped GaN buffer layer followed by a doped

<sup>a)</sup>Electronic mail: [srajan@ece.ucsb.edu](mailto:srajan@ece.ucsb.edu)

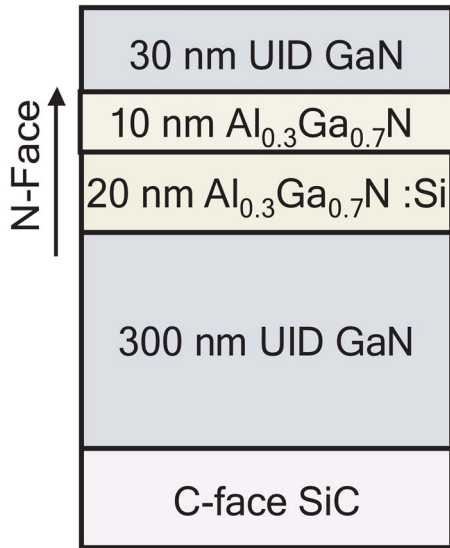


FIG. 1. (Color online) Epitaxial layer structure of N-polar GaN/AlGaN/GaN HEMT.

$\text{Al}_{0.3}\text{Ga}_{0.7}\text{N}$  barrier, an  $\text{Al}_{0.3}\text{Ga}_{0.7}\text{N}$  spacer, and a GaN cap, as shown in Fig. 1. Modulation doping was used to ensure that the 2DEG charge at the upper  $\text{Al}_{0.3}\text{Ga}_{0.7}\text{N}/\text{GaN}$  interface was insensitive to changes in the GaN cap surface due to processing and air exposure. The Si concentration in the modulation-doped region was estimated from secondary ion mass spectroscopy (SIMS) calibrations on GaN to be  $2 \times 10^{18} \text{ cm}^{-3}$ .

The band diagram of this structure is shown in Fig. 2. The device fabrication in the case of N-polar material required changes to the standard processing recipes used in Ga-polar high electron mobility transistor (HEMT) processing. Since N-polar GaN etches in developer, Ge was used as a sacrificial layer to prevent etching of the epitaxial layers during processing. The Ge was etched away using 1:3 dilute  $\text{H}_2\text{O}_2$ , which does not attack N-polar GaN. Ohmic contact optimization was carried out since the Ohmic contact resistance using the optimal layer thickness for Ga-polar HEMTs [Ti/Au/Ni/Au (20/120/30/50 nm)] was found to be  $2 \Omega \text{ mm}$ , which is very high. The optimal layer stack was Ti/Au/Ni/Au (20/100/10/50 nm), and a rapid thermal anneal for 30 s at  $870^\circ \text{C}$  in  $\text{N}_2$  ambient was carried out, yielding an acceptable low contact resistance of  $0.4 \Omega \text{ mm}$ .  $\text{Cl}_2$ -based reactive ion etching was used to carry out mesa

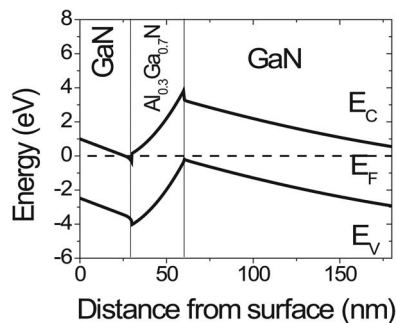


FIG. 2. Energy band diagram of N-polar GaN/AlGaN/GaN HEMT.

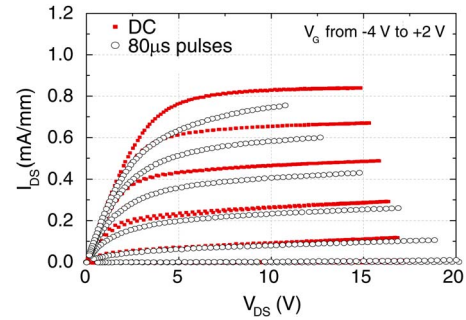


FIG. 3. (Color online) dc and pulsed  $I$ - $V$  characteristics of N-polar GaN/AlGaN/GaN transistor. There is significant dispersion under pulsed conditions.

isolation, Ni/Au/Ni (30/300/30 nm) gate contact layers were deposited. Both steps used conditions similar to Ga-polar HEMT fabrication.

## B. Device characterization

Field effect transistors with a gate length of  $0.7 \mu\text{m}$  and a source-drain spacing of  $3.4 \mu\text{m}$  were fabricated. Transfer length method (TLM) measurements were carried out and a sheet resistance of  $550 \Omega/\square$  was measured with a contact resistance of  $0.4 \Omega \text{ mm}$ . The Hall charge and mobility on these samples were  $1 \times 10^{13} \text{ cm}^{-2}$  and  $1400 \text{ cm}^2 \text{ V}^{-1} \text{ s}^{-1}$ , respectively. Buffer leakage was measured using isolation test patterns, where the channel region between the source and drain was etched away. The buffer leakage in these structures was low, with a  $4 \text{ mA/mm}$  leakage current measured at source-drain bias of  $80 \text{ V}$ . Representative dc  $I$ - $V$  data carried out using a Tektronix 370A curve tracer are shown in Fig. 3. A maximum current of  $800 \text{ mA/mm}$  was measured, with a pinch-off voltage of  $-4 \text{ V}$ . An HP 4155 parameter analyzer was used to measure the extrinsic transconductance. At a drain bias of  $10 \text{ V}$ , the peak transconductance of these devices was  $195 \text{ mS/mm}$ . Small-signal high frequency characterization was carried out on these samples using on-wafer probes and an Agilent 8263a network analyzer. The dependence of  $f_T$  and  $f_{\text{MAX}}$  on the drain current at a drain bias of  $20 \text{ V}$  is shown in Fig. 4. A peak  $f_T$  of  $18 \text{ GHz}$  and  $f_{\text{MAX}}$  of  $44 \text{ GHz}$  was measured. The gate length- $f_T$  product ( $12.6 \text{ GHz } \mu\text{m}$ ) is similar to that in typical Ga-face

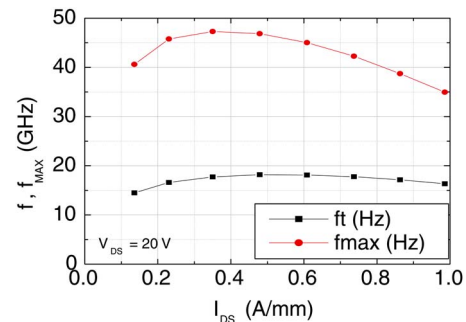


FIG. 4. (Color online) Small-signal high frequency characteristics of N-polar GaN/AlGaN/GaN transistor.

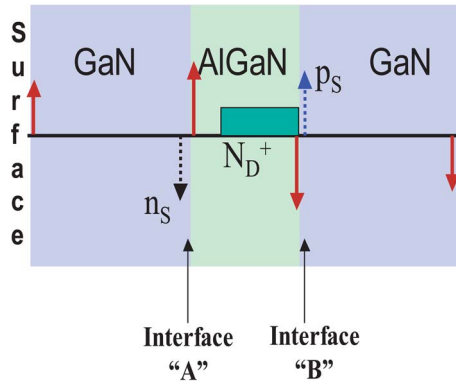


FIG. 5. (Color online) Schematic showing the different charges in N-polar GaN/AlGaIn/GaN HEMTs.

AlGaIn/GaN HEMTs with similar gate lengths. The small-signal performance of these transistors is the best ever reported so far for N-polar GaN FETs.

Pulsed measurements were carried out to investigate large-signal dispersion in the samples. Gate pulses from 1 V below pinch-off with a width of 80  $\mu$ s were applied along a 50  $\Omega$  load line. As shown in Fig. 3, significant dispersion was observed in the transistors. The transistor  $I$ - $V$  curves were also found to be sensitive to light, suggesting that the dispersion was not caused by surface states, but by states within the device structure.

### III. ELIMINATION OF BULK TRAP DISPERSION

#### A. Bulk traps and dispersion

The charge profile in the HEMT structure is shown in Fig. 5. In the figure,  $p_s$  is the positive charge at the bottom GaN/AlGaIn interface,  $N_D$  is the modulation doping density, and  $n_s$  is the electron sheet charge density at the top AlGaIn/GaN interface. Schrodinger-Poisson simulations were carried out for the structure at different gate biases in order to find the positive and negative sheet charge densities ( $p_s$  and  $n_s$ ) at each bias. These are shown in Fig. 6. The depletion charge due to the Si dopants remains constant. As the gate bias is made more negative, the channel pinches off, and  $n_s$  drops to zero. At the same time,  $p_s$  increases after pinch-off due to the negative gate bias. In the simulations, the positive charge was due to holes at the GaN/AlGaIn interface. However, holes have not been obtained in GaN-based heterostructures in the absence of  $p$ -type doping.<sup>6,7</sup>

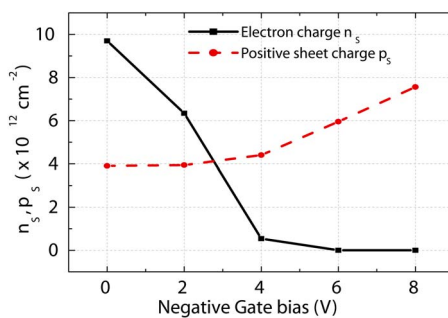


FIG. 6. (Color online) Simulated positive sheet charge as a function of bias. The simulations were carried out using BANDENG (Ref. 10).

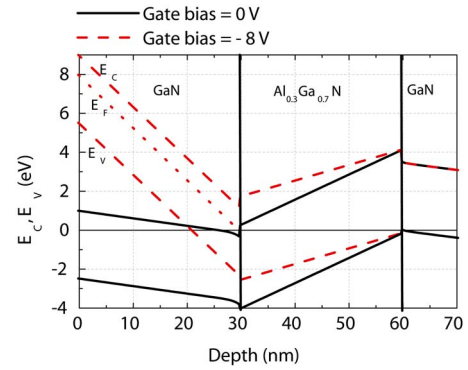


FIG. 7. (Color online) Band diagram of GaN/AlGaIn/GaN structure at equilibrium and below pinch off.

Deep level capacitance transient spectroscopy (DLTS) measurements on N-polar and Ga-polar structures have shown a donorlike state approximately 60 meV from the valence band at GaN/AlGaIn interfaces with negative polarization charge.<sup>8</sup> Band diagram simulations were carried out using deep donor traps at the bottom AlGaIn/GaN interface, and it was found that the positive charges that were attributed to holes in the earlier simulations could also be due to positively charged donor states. Therefore, we consider it likely that the positive charges at the GaN/AlGaIn interface are due to donorlike trap states.

The band diagram of the GaN/AlGaIn/GaN structure for a surface barrier  $V_G$  of 0 V is shown in Fig. 7. The Fermi level is close to the valence band edge at the bottom GaN/AlGaIn interface  $B$ , and the positive charges are induced due to ionization of the trap states. We now propose a mechanism for dispersion in these transistors. When the transistor is in pinch-off, such as the  $V_G=8$  V point in the curve, the magnitude of the positive charge increases, reducing the magnitude of the electric field in the AlGaIn. As a result, relative to the Fermi level at the bottom GaN/AlGaIn interface  $E_f(B)$ , the conduction band in the AlGaIn/GaN interface is now higher than at the  $V_G=0$  V bias. This is shown in Fig. 7. Now the gate bias is changed so that the surface barrier changes from 8 V back to the on condition, or 0 V. Since the donor traps do not respond immediately, the field in the AlGaIn does not change. Since there are still no electrons in the channel, the field in the GaN remains the same as in the pinch-off condition. The Fermi level position relative to the conduction band is determined by the donor states at the bottom ( $B$ ) interface, and therefore the conduction band is still above the Fermi level. As a result, no degenerate electron gas can be formed. When the donor states capture electrons and reach the equilibrium ionized concentration, the electric field is returned to the stable value, and an electron distribution is formed. However, since the donor states respond slowly, there is a time lag before the electron concentration reaches its full value, and this causes dispersion in the transistor.

#### B. Design of Si-doped graded AlGaIn back barrier

The physical nature of the defects that behave as donor traps and cause current collapse in the earlier section is not

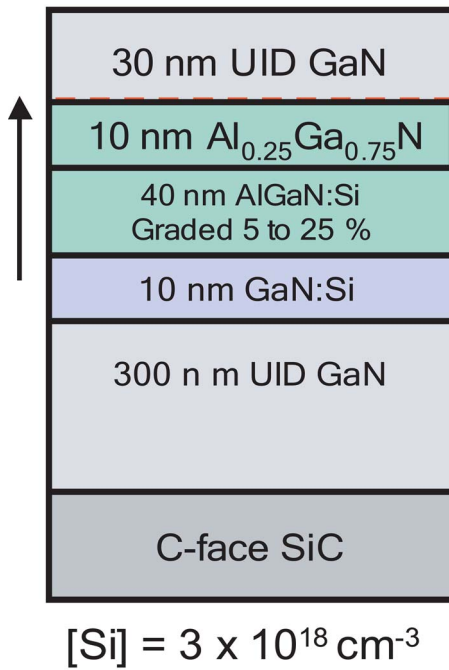


FIG. 8. (Color online) Epitaxial structure of N-polar GaN/graded AlGaIn/GaN HEMT for reduced dispersion.

known. The defects could be located at the AlGaIn/GaN interface or in the bulk AlGaIn, and further studies are needed to investigate this further. These states have been seen to appear in both Ga-polar and N-polar devices, where a negative polarization sheet charge is encountered.<sup>6,9</sup>

However, as shown in the earlier section, the reason for the current collapse is that the trap ionized charge density is modulated during normal operation of the transistor. Since the trap level is close to the valence band, and the valence band in the earlier GaN/AlGaIn/GaN structure was also close to the Fermi level, perturbations to the gate potential led to modulation of charge density. In order to eliminate the modulation of traps, a structure was designed where the Fermi level was kept away from the valence band (and the trap level). The epitaxial structure is shown in Fig. 8. It consists of an undoped GaN buffer followed by 10 nm GaN:Si, 5%–25% AlGaIn graded linearly over 40 nm, a 10 nm Al<sub>0.25</sub>Ga<sub>0.75</sub>N layer, and a 30 nm GaN channel layer. The curvature from the positively charge Si donors in the graded region helps to keep the Fermi level position away from the valence band in the entire structure. The same technique has been used in deep-recess HEMT structures.<sup>9</sup> The band diagram calculated using BANDENG (Ref. 10) is shown in Fig. 9. The valence band in this structure is kept far away from the Fermi level to ensure that there is no modulation of trap levels or holelike states near the valence band.

### C. Growth and device characterization

The structure shown in Fig. 8 was grown by plasma-assisted MBE. The dependence of the Al composition in Al-GaN alloys on the Al flux (measured using a beam flux monitor) for N-polar growth was calibrated using x-ray measurements. The temperature of the Al cell in the MBE growth chamber was then varied to obtain a linearly varying Al flux

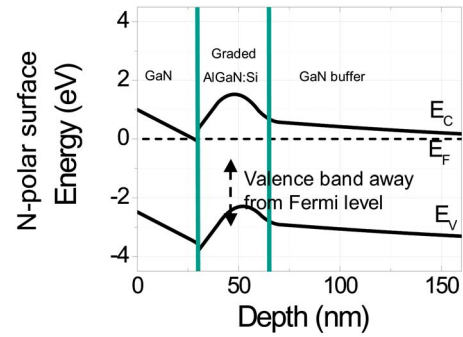


FIG. 9. (Color online) Energy band diagram of N-polar GaN/graded AlGaIn/GaN HEMT for reduced dispersion.

that corresponded to the graded layer design specifications. A piecewise linear grade was used to approximate the actual continuous grading profile, and the points in the piecewise linear function were spaced by 1 nm. To ensure that no overshoot or undershoot effects were taking place in the Al cell flux response, the Al flux was measured for the actual grading profile.

The Si doping levels were estimated using SIMS calibrations on GaN samples as a reference. Hall measurements were carried out on the sample on van der Pauw patterns, and the charge and mobility were found to be  $7.5 \times 10^{12} \text{ cm}^{-2}$  and  $1400 \text{ cm}^2 \text{ V}^{-1} \text{ s}^{-1}$ , respectively. Field effect transistors were fabricated using the graded AlGaIn design. The dc and pulsed  $I$ - $V$  measurements from a typical device are shown in Fig. 10. The pulsed measurements were taken by pulsing the gate voltage from 1 V below pinch-off to successively higher gate voltages in steps of 1 V, at each drain bias. The pulse width was 200 ns, and the duty cycle was 10%. As seen in the curves, very little current collapse or knee walk-out is seen. Also, the  $I$ - $V$  curves were found to be almost insensitive to light, unlike the abrupt N-polar GaN/AlGaIn/GaN transistors. Small-signal characterization was also carried out on the samples, and the peaks  $f_T$  and  $f_{\text{MAX}}$  of the measured devices were 17 and 36 GHz, respectively.

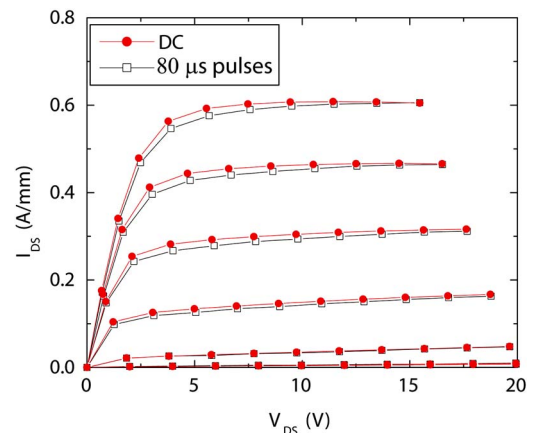


FIG. 10. (Color online) dc and pulsed  $I$ - $V$  curves for GaN/graded AlGaIn/GaN HEMT. The gate voltage was varied from  $-5$  to  $0$  V. There is very little dispersion under pulsed conditions. The poor pinch-off was due to the high gate leakage in the devices.



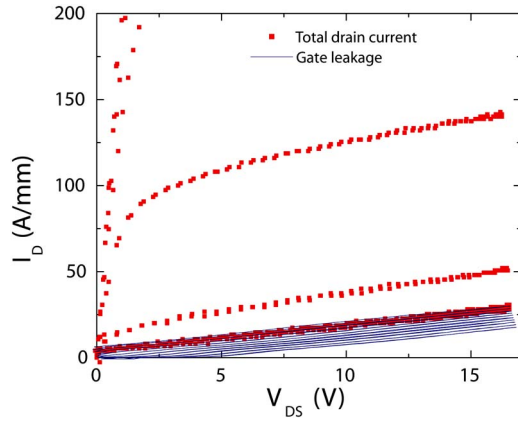


FIG. 11. (Color online) dc three-terminal current and two-terminal gate current in a GaN/graded AlGaIn/GaN HEMT. The figure shows that the bulk of the three-terminal leakage current can be attributed to gate leakage.

The gate leakage in these samples was very high, with two-terminal gate-drain breakdown of 4 mA/mm occurring below 20 V. This causes degradation in pinch-off of the transistor, as shown in Fig. 11 where the gate-drain leakage (with source open) is plotted together with the transistor drain current. The maximum gate current curve (at the most negative gate bias) makes up the bulk of the three-terminal transistor leakage. There are many possible reasons for the high gate leakage. First, since the cap layer in these devices is GaN, the Schottky barrier height for the gate is low, and therefore the leakage is higher. Second, in addition, due to the doping in the back barrier in N-polar devices, the total fixed charge is much higher than in Ga-polar devices with the same AlGaIn barrier composition, thus leading to higher peak fields and earlier breakdown. Finally GaN has a low breakdown field compared to AlGaIn. Since there is a relatively thick GaN layer with a high field, these devices could be expected to suffer impact ionization breakdown at a lower voltage compared to AlGaIn/GaN HEMTs. A combination of these effects causes a decrease in the gate-drain breakdown voltage of devices.

#### IV. AlGaIn-CAP N-POLAR DISPERSION-FREE HEMTS

To reduce the gate leakage in these devices, structures with AlGaIn caps on top of the GaN channel were designed. The use of an AlGaIn-cap layer is expected to improve the breakdown voltage due to several reasons. First, since the Schottky barrier height is much higher on AlGaIn than on GaN, the gate leakage is expected to be lower. Second, keeping the GaN channel layer thin helps reduce the impact ionization in the device under high breakdown fields. Finally, a negative polarization sheet charge in the top AlGaIn/GaN interface near the channel reduces the effective lateral electric fields in the devices. However, the design space of the AlGaIn-cap HEMT is restricted. The bottom AlGaIn/GaN interface has a negative polarization sheet charge that depletes the charge in the GaN. Therefore, to obtain a reasonable charge density, the composition and thickness of the cap cannot be too high. Finally, it is important to design the structure so that the valence band at the bottom AlGaIn-cap/GaN interface does not approach the Fermi level during de-

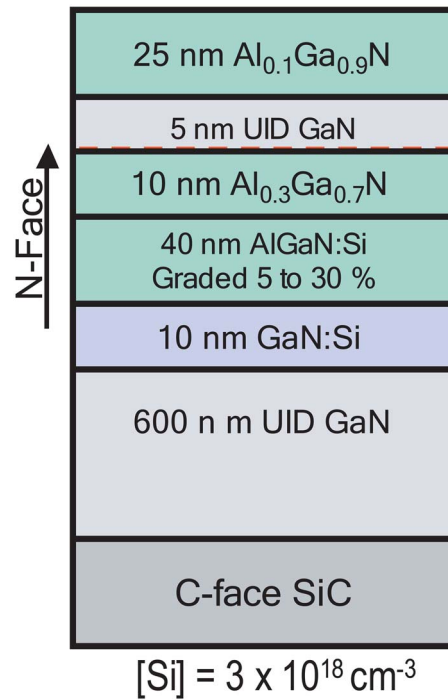


FIG. 12. (Color online) Epitaxial structure of AlGaIn-cap N-polar HEMT.

vice operation. As discussed earlier, the trapping effects at this interface can cause significant current collapse and dispersion.

Taking into account the device design considerations described in the earlier section, a device epilayer was designed and is shown in Fig. 12. Figure 13 shows the equilibrium band diagram of the structure. The active layer consisted of a graded AlGaIn back-barrier, a 5 nm GaN channel, and a 25 nm  $\text{Al}_{0.1}\text{Ga}_{0.9}\text{N}$  cap. The Hall charge and mobility in this sample were  $6 \times 10^{12} \text{ cm}^{-2}$  and  $1200 \text{ cm}^2 \text{ V}^{-1} \text{ s}^{-1}$ , respectively. The back-barrier had the same design as described in Sec. III. Gate leakage was found to be much lower on these samples, and the two-terminal gate-drain breakdown was 70 V (for a leakage current of 4 mA/mm). Small-signal characterization was carried out on these samples, and the  $f_T$  and  $f_{\text{MAX}}$  were 14 and 35 GHz respectively. The lower  $f_T$  and  $f_{\text{MAX}}$  compared to the Ga-polar HEMTs are attributed to the relatively high sheet resistance in these samples compared to state-of-art devices.

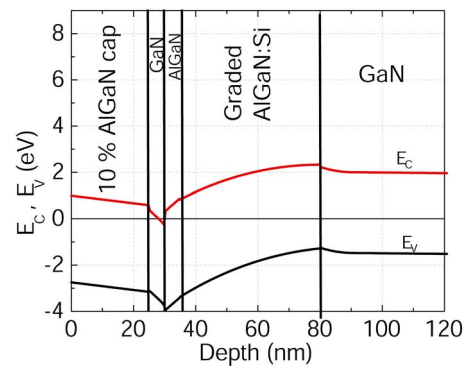


FIG. 13. (Color online) Equilibrium band diagram of AlGaIn-cap N-polar HEMT.

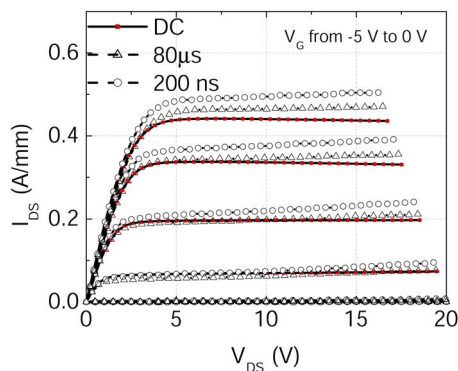


FIG. 14. (Color online) dc and pulsed  $I$ - $V$  characteristics of AlGaIn-cap N-polar HEMT. The gate voltage was varied from  $-5$  to  $0$  V. No dispersion was observed under pulsed conditions.

Figure 14 shows the dc and pulsed  $I$ - $V$  performance of this device. The  $200$  ns and  $80$   $\mu$ s pulsed currents were higher than the dc currents indicating minimal dispersion. Therefore, a low-dispersion device with a low gate leakage was achieved on N-polar GaN.

## V. CONCLUSIONS

The work described in this chapter shows that N-polar material of high electrical quality can be grown on C-face SiC using  $N_2$  plasma-assisted molecular beam epitaxy. A two-step buffer scheme was developed to achieve films with high structural quality and smooth surfaces. AlGaIn/GaN heterostructures were grown on N-polar material, and their properties were found to match theoretical predictions. Device fabrication techniques were developed, and field effect

transistors were fabricated on N-polar material. Dispersion due to hole traps was understood and eliminated. Finally, the gate leakage in these transistors was reduced by using a quantum-well channel with an AlGaIn cap. Devices with low dispersion and high three-terminal breakdown voltages were achieved. The knowledge base of N-polar FET physics and technology developed in this work can be applied to further improve these devices, and to address problems where the unique properties of N-polar GaN provide a solution.

## ACKNOWLEDGMENTS

The authors would like to thank Michael Grundmann for the use of Schrodinger-Poisson simulator, BANDENG. The authors are grateful to Likun Shen and Christiane Poblentz for helpful discussions. The authors gratefully acknowledge funding from AFOSR (Program managers: Gerald Witt and Kitt Reinhardt) and the DARPA CNID program.

<sup>1</sup>R. Dimitrov, M. Murphy, J. Smart, W. Schaff, J. R. Shealy, L. F. Eastman, O. Ambacher, and M. Stutzmann, *J. Appl. Phys.* **87**, 3375 (2000).

<sup>2</sup>M. J. Murphy *et al.*, *MRS Internet J. Nitride Semicond. Res.* **4S1**, G8.4 (1999).

<sup>3</sup>K. Xu and A. Yoshikawa, *Appl. Phys. Lett.* **83**, 251 (2003).

<sup>4</sup>S. Rajan, A. Chini, M. Wong, Y. Fu, F. Wu, J. S. Speck, and U. K. Mishra, *Jpn. J. Appl. Phys., Part 2* **44**, L1478 (2005).

<sup>5</sup>P. Waltereit, C. Poblentz, S. Rajan, U. K. Mishra, and J. S. Speck, *Jpn. J. Appl. Phys., Part 2* **43**, L1520 (2004).

<sup>6</sup>M. Grundmann, Ph.D. Thesis, University of California, 2007.

<sup>7</sup>P. Kozodoy *et al.*, *Appl. Phys. Lett.* **75**, 2444 (1999).

<sup>8</sup>A. Chini, Y. Fu, S. Rajan, J. S. Speck, and U. K. Mishra, 32nd International Symposium on Compound Semiconductors (ISCS), Europa-Park Rust, Germany, 18–22 September 2005 (unpublished).

<sup>9</sup>L. Shen, Ph.D. thesis, University of California, 2004.

<sup>10</sup>M. Grundmann, BANDENG, 2005, <http://michaelgrundmann.com>

Journal of Applied Physics is copyrighted by the American Institute of Physics (AIP). Redistribution of journal material is subject to the AIP online journal license and/or AIP copyright. For more information, see <http://ojps.aip.org/japo/japcr/jsp>